

# Influence of near-leading edge curvature on the performance of aero-engine intake lips at high-incidence

A. Coschignano\* and H. Babinsky†

*Department of Engineering, University of Cambridge, Cambridge, CB2 1PZ, UK*

C. Sheaf‡ and E. Platt‡

*Installation Aerodynamics, Rolls Royce Plc., Derby, DE24 8BJ, UK*

This paper describes the investigation into the flow over the lip of subsonic engine intakes at incidence, focusing on the shock wave-boundary layer interaction occurring over the inner lip. A baseline geometry is considered along with two variations, characterised by a sharper and a blunter intake highlight (i.e.: nacelle leading edge) respectively. Results to date reveal a relatively benign interaction for the baseline model, with small or no shock-induced separation reported under on-design conditions, which correspond to typical take-off or climb circumstances. The alternative geometries reveal a considerable influence of near-highlight curvature on the flow development. In particular, a blunter nose leads to the formation of a larger supersonic region, terminated by a consequently stronger shock, which shows a greater degree of shock-induced separation and increased total pressure losses and unsteadiness. The sharp nose, on the other hand, resulted in the compression occurring via three separate shock-waves, all of which weak. Overall, none of the three intake geometries showed inherently unsteady behaviour. However, this is expected to occur as the engine flow demand increases. Further testing is in progress to assess off-design performance and to produce a complete operational envelope for intakes at incidence.

## Nomenclature

$\kappa$	Surface curvature
$\rho$	Density
$\dot{m}$	Mass flow
$m_x$	Modified super ellipse $x$ exponent
$n$	Modified super ellipse $y$ exponent
$a$	Modified super ellipse major axis
$b$	Modified super ellipse minor axis
$U$	flow velocity
$M$	Mach number
$P$	Static Pressure
<i>Subscript</i>	
0	Property upstream of the shock - Stagnation value
1	Property at the tunnel entry
<i>Abbreviations</i>	
$AR$	Intake aspect ratio
$LDV$	Laser Doppler Velocimetry

---

\*PhD Student, Department of Engineering, University of Cambridge, AIAA Student Member.

†Professor of Aerodynamics, Department of Engineering, University of Cambridge, AIAA Associate Fellow.

‡Installation Aerodynamics, Rolls Royce Plc, Derby.

# I. Shock-Boundary Layer Interactions in Subsonic Engine Intakes

When travelling at an incidence, such as during take-off and climb, the substantial mass flow demand by a turbofan engine is sufficient to accelerate the flow over the intake lip to supersonic conditions. This faster-than sound flow pocket is terminated by a near-normal shock wave. The adverse pressure gradient imposed by this disturbance on the boundary layer can cause the latter to separate, introducing large scale unsteadiness and an increase in viscous losses. These losses have a direct negative repercussion on the overall engine efficiency as the total pressure reaching the fan face is reduced. Moreover, if the separated boundary layer does not reattach before the engine face, the unsteadiness, characteristic of separated flows, may increase the stress on the fan, which can ultimately reduce component lives. A schematic representation of the typical flow structure developing over an intake cross section is shown in Figure 1.

Although a significant amount of research has gone into reducing the detrimental effects associated with shock-induced separation in transonic flight, the majority of these efforts have been limited to aerofoil design. In fact, the formation of shock waves on the inside lip of engine intakes has often been overlooked and thus there is insufficient understanding and a lack of data for CFD validation. Recently, engine manufacturers are moving towards larger engines and opting for slimmer nacelles to enhance overall efficiency.<sup>1</sup> The reason for the latter is to be found in the reduced wetted area and, consequently, reduced drag. However, slimmer intake lips naturally imply higher curvature near the leading edge, which may result in greater flow acceleration and ultimately leading to stronger shocks. The consequences of novel design choices on the nature of the interaction between the shock and the boundary layer is yet to be investigated, as the few parametric studies performed on engine intakes to date were limited to purely incompressible flows.

The research currently undertaken at Cambridge University Engineering Department (CUED) not only assesses the viability of a slimmer nacelle, but also investigate the response of shock-boundary layer interactions (SBLIs) to geometry changes. The scope of this paper is to present the effect of near-leading edge curvature on the flow-field over the inlet lip and its effect on the SBLI. Ideally, this will result in useful design criteria for next-generation engine intakes, which will not only satisfy the novel thickness requirements, and thus reduce parasitic drag by design, but also minimise the stagnation pressure losses and unsteadiness related to compressibility effects.

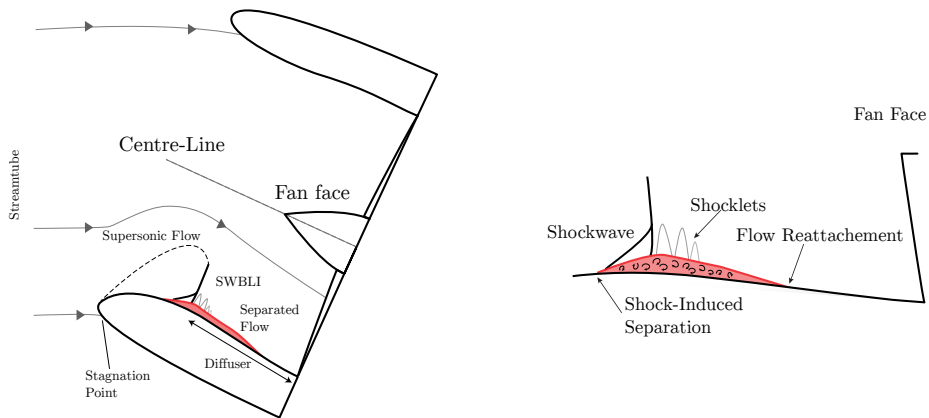


**Figure 1. Schematic representation of shock-induced boundary layer separation over an intake lip cross-section during high-incidence flight.**

## II. Experimental set-up and methodology

### A. Experimental facility

All experiments are performed at the high-speed aerodynamics laboratory at the University of Cambridge. In particular, a blow-down wind tunnel, powered by two 50 kW compressors, is used. The flow is fed from the compressors into the settling chamber, where it is passed through a number of flow straighteners and turbulence grids before going through a 18:1 contraction. In the current configuration, no nozzle is used

and the entry velocity is varied by changing the stagnation pressure and the effective area of the second throat where the flow is choked. By altering the cross-sectional area of the second throat by means of an aerofoil (see Figure 2) the overall mass flow rate is adjusted, controlling the entry Mach number with an accuracy of  $\pm 0.001$ . The working section was designed by Makuni<sup>2</sup> exclusively for the investigation of shock wave boundary layer interactions in engine intakes. The working section is depicted in Figure 2 and features curved upper and lower walls, forming a stream-tube divided by a  $1/7^{th}$  scale intake lip model. The stream-tube design is based on computational results performed for a real intake.<sup>2</sup> The upper boundary is a streamline of the computed flow far enough from the supersonic region to avoid choking in the upper channel. The mass flow rate into the lower channel is controlled by choking the flow with an adjustable plug as indicated in Figure 2. For a given stagnation pressure, by manually reducing the lower channel area, more mass flow is forced into the upper channel mimicking a greater mass flow demand by the engine. As the ratio between the upper and lower channel mass flows increases, the stagnation streamline is lowered, resulting in stronger acceleration and thus a greater supersonic region. This allows the assessment of performance at off-design conditions.

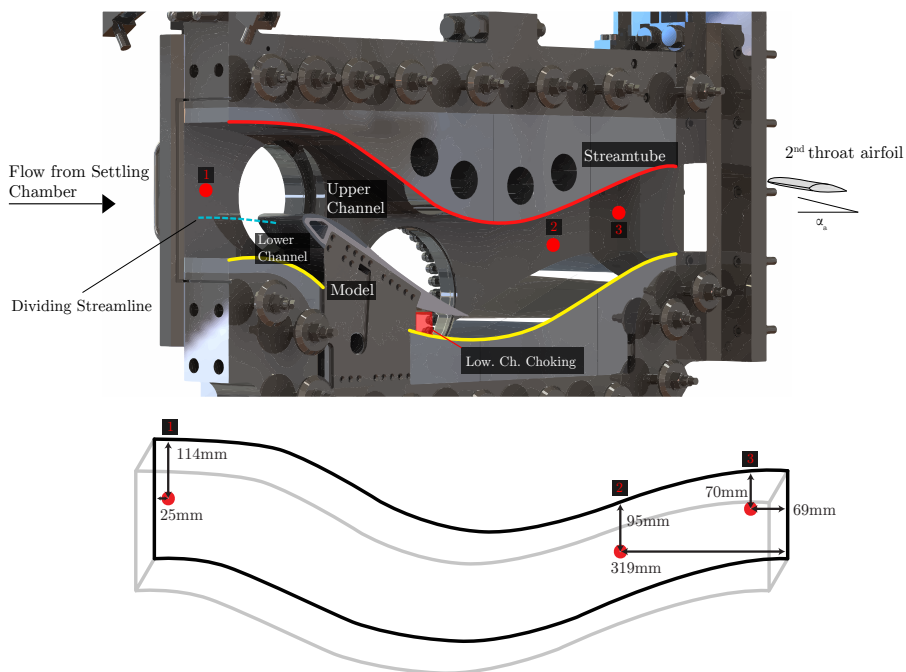


**Figure 2.** Representation of the blow-down wind tunnel working section. Stream-tube designed based on computed flow streamlines. The position of the three points where pressure measurements are taken are highlighted in red. Tunnel entry Mach number is measured at the location of Port No.1 and so was free stream turbulence

The experimental operating range is portrayed in Figure 3. The rig is capable of achieving entry conditions of  $M_1 = 0 \rightarrow 0.45$ , for  $\alpha$  up to 29 degrees. The characteristic length used for calculating the Reynolds number is the maximum intake lip thickness. In the range  $M_1 = 0.25 \rightarrow 0.45$ , the experiment is capable of matching full scale Reynolds numbers for altitudes greater than 5000ft and 25000ft for a small and large engine respectively. The highest supply pressure possible is 2.4 bar.<sup>2</sup> A pair of windows on each side of the working section allows high speed Schlieren photography and estimation of static wall pressure over the intake cross-section by exploiting the properties of pressure sensitive paint (PSP).

The settings listed in Table 1 result in a flow field closely matching the target flow provided by both experiments and Rolls Royce computational efforts based on a real intake travelling at a free-stream Mach number of 0.3 and representative angle of attack, typical for take-off conditions. The wind-tunnel free stream turbulence was measured using a hot wire at the tunnel entry. For  $M_1 = 0.435$ , the turbulence level was found to be  $< 1\%$ .

The boundary layer displacement thickness upstream of the shock could not be measured directly by

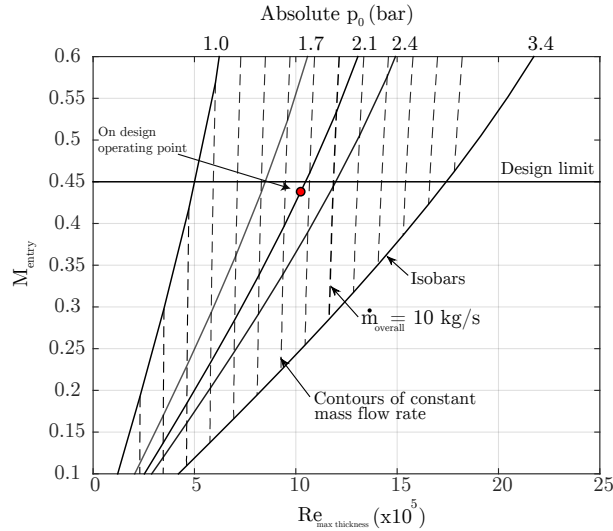


**Figure 3.** Wind tunnel operational envelope in terms of entry Mach number (or equivalently mass flow rate). Adapted from Makuni.<sup>2</sup>

**Table 1.** Tunnel entry conditions for on-design investigation

$\dot{m}$ (kg/s)	$M_1$	AoA (deg.)	$P_0$ (kPa)	$T_0$ (K)	$I_{\%}$
8.68	0.435	23	211.6	290±4	0.88

LDV due to poor data rate in the immediate proximity of the wall. From qualitative data observation, this is estimated to be  $<0.2\text{mm}$ . This is particularly important when determining the effective aspect ratio of experimental facilities and assessing the impact of corner flows on centre span separation. According to the findings by Bruce et al.,<sup>7</sup> the resulting  $\delta^*/w$  ratio, where  $w$  is the tunnel width (114mm for the CUED facility), would suggest the absence of strong 3D effects and the corner flows are, thus, not expected to affect the onset of shock-induced separation in the centre-span. Further support to this hypothesis will be considered when discussing experimental results.

A number of different techniques is used to investigate the flow. In particular, a Schlieren technique is used to visualize the features typical of supersonic flows such as shock waves. A light source is placed at the focus of a mirror, which produces collimated light that is passed through the tunnel working section, where changes in density occurs as a consequence of compressibility effects in the transonic regime. The light is then collected by a second mirror that focuses all the rays. However, the density gradients within the working section have produced a deflection of some of the rays. As a result, these will not be concentrated at the focal point. A knife edge is placed here to intercept some of the rays, while other will go through without being obstructed. This ultimately results in dark patches where the beams were blocked by the obstruction and brighter patches where the rays deviated by the density gradients were not intercepted by the knife edge. In such a system, the resulting light intensity is proportional to the first derivative of the light retardation, allowing the visualization of shock waves, as well as expansion and compression waves.<sup>3</sup>

Pressure measurements are taken during the run to both characterise the flow and to assess the experimental repeatability. These measurements are obtained by using pressure taps drilled along the surface of the intake model and connected via tubing to a differential pressure transducer. Furthermore, a number of these pressure readings are used to calibrate pressure sensitive paint. The photons reflected when the latter is excited by UV light are directly proportional to the pressure acting on it. An optical device is used to measure such luminescence, resulting in a number of pressure readings equivalent to the camera resolution available. The relationship between luminescence intensity and pressure is determined by the Stern-Volmer

relation:<sup>4</sup>

$$\frac{I_{ref}}{I_{(P,T)}} = A(T) + B(T) \frac{P}{P_{ref}} \quad (1)$$

$I_{ref}$  is the luminescence taken at a reference pressure and temperature. The obvious choice is to measure the intensity at normal atmospheric conditions with the tunnel off. A second image is taken with the flow on. A no flow - no light background image is subtracted to both images to reduce noise from external light sources. Finally, accordingly to the Stern-Volmer equation, the flow-off reference image is divided by the flow-on image to obtain the pressure ratio. By using the pressure taps located on the model, the values of the constants  $A(T)$  and  $B(T)$  can be determined and the absolute pressure values can be extracted from raw light intensity. To minimise the calibration error, estimated to be  $<2\%$  for a typical calibration curve in the current investigation, 5-6 points are required.<sup>4</sup> Given the rig configuration and the position of the access windows, the images are captured at an angle and are, thus, characterised by severe prospective distortion. For this reason, along with the fact that, due to the curved nature of the intake, extracting pressure readings along the surface requires the photo to be flattened, all the PSP images have been processed via the same un-warping algorithm and will be presented as a two dimensional contour plots.

Furthermore, streak-lines are visualised by means of a dense mixture applied on the model prior to the run. This results in the skin-friction lines being deposited on the surface, offering an accurate depiction of the flow structures. Shock waves will cause an accumulation of oil near the foot. Similarly, the stagnation point will be characterised by greater oil residuals. Most importantly, this technique becomes extremely valuable when determining the extent of shock induced separation. In fact, the flow recirculation, typical of separated boundary layers, is captured by the oil mixture. The mixture is a combination of Titanium Dioxide ( $\text{TiO}_2$ ) powder, used as a pigment, and Kerosene (or paraffin), ideal for its low kinematic viscosity. Generally, a small amount of oleic acid is added to improve the mixing and reduce the coagulation of  $\text{TiO}_2$  powder.

Finally, direct velocity measurements are taken by using Laser Doppler Velocimetry (LDV). A two component LDV system by TSI is used. Two pairs of coherent laser beams, with a wavelength of 542nm and 532nm respectively, are focused inside the working section to form the interference pattern of the ellipsoidal working volume, measuring  $130\mu\text{m}$  in diameter. Kerosene particles, with a diameter of approximately  $0.5\mu\text{m}$ , are used to seed the flow and allow velocity measurements to be recorded via a proprietary software. The laser emitting head and receiving optics are mounted on a traverse capable of moving in one direction with a user defined velocity. Typical measurement accuracy is  $\pm 0.1\%$  of  $U_{max}$  ( $\sim 580\text{m/s}$ ).

Stagnation temperature is recorded by using 4 T-type thermocouples placed in the settling chamber. A linear drop of stagnation temperature from  $\sim 294\text{K}$  to  $\sim 286\text{K}$  is recorded during an average 30 second long run. This variation in stagnation temperature is taken into account when converting absolute velocity measurements from LDV to local Mach number to minimise the error involved, which would otherwise peak  $1.7\%$ .

## B. Intake Lip Design

The intake lips considered here have been designed by using a modified super ellipse profile. Mathematically, a super ellipse is defined as:

$$\left(\frac{x-a}{a}\right)^m + \left(\frac{y}{b}\right)^n = 1 \quad (2)$$

where  $a$  and  $b$  are the major and minor axis of the ellipse, respectively controlling the position and the size of the ellipse highest point. In intake terms, such point indicates where the intake is at its thickest, i.e.: the throat. The ratio  $\frac{a}{b}$  is defined as the aspect ratio  $AR$  of the ellipse. The powers  $m$  and  $n$ , on the other hand, set the locus of the point of maximum curvature with smaller values associated to sharper noses. Moreover, to reduce the number of parameters involved in the geometry definition, a modified super ellipse (MSE) approach was preferred for the current parametric study as used by Lin<sup>5</sup> and Schrader,<sup>6</sup> amongst many, for their flat plate boundary layers investigations. A modified super ellipse is defined similarly to Equation (2). However, to further reduce the number of variables,  $m$  is not chosen arbitrarily, but varies between 2 and 3 along the major axis of the ellipse according to the equation:<sup>5</sup>

$$m(x) = 2 + \left(\frac{x}{a}\right)^2 \quad (3)$$

Combining Equation (2), (3) and keeping the aspect ratio constant, a number of modified elliptical profiles can be obtained, defining a family of curves for different values of the exponent  $n$  only. This type of ellipse results in a continuous reduction in curvature, which falls to zero at the point of maximum thickness. This characteristic has made the super ellipse a good candidate for leading-edge design of flat plates or other similar purposes where a continuous curvature distribution is required.<sup>5</sup> However, if an subsonic engine intake is considered, it is noted that, at the point of maximum thickness (i.e.: the intake throat), the curvature does not drop to zero but the surface simply changes concavity. After this point, beyond which a super ellipse is not defined, the intake lip is smoothly connected, by means of a bridge spline, to the rest of the inner intake, which uniformly decelerates the flow in the diffuser section. This is done by forcing the first two derivatives to match at the joint between the front and the rear part of the intake model. Figure 4 shows how the parameters defined in Equation (2) relate to the design of a real intake lip. The baseline geometry is defined by a modified super ellipse of aspect ratio  $AR < 3$  and a value of  $n = 1.98$ . Figure 4 also shows a plot of the theoretical curvature distribution along the surface of the three lips considered in the current investigation. Note that the term *leading edge* and *highlight*, referring to the intake models, are used interchangeably in the following paper.

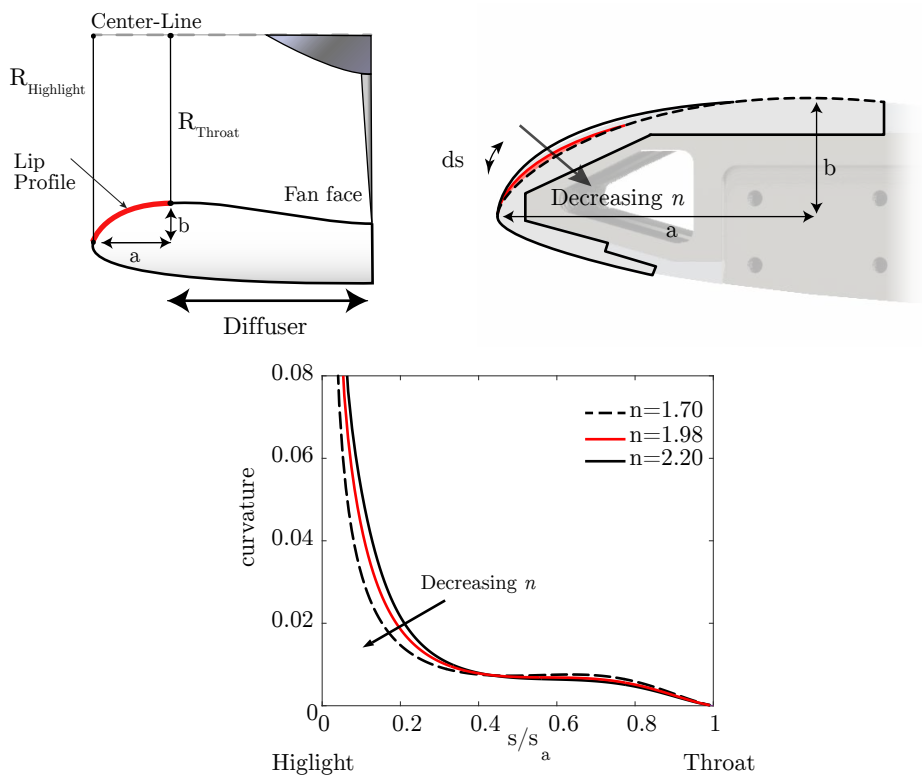


Figure 4. Variation in curvature distribution along the nacelle lip upper surface for decreasing highlight bluntness.

### III. Results

#### A. Baseline Flow

As aforementioned, the target flow was provided by validated computations performed on 3D intakes. The stagnation pressure achieved in the wind tunnel, equivalent to 2.1bar, results in a Reynolds number of  $\sim 10^6$ , representative of a medium size engine at take off. The area ratio between the second throat and the tunnel entry was chosen to give a Mach number at the tunnel entry of 0.435. The latter is set with an accuracy of  $\pm 0.001$  and was determined based on computations. Furthermore, the stagnation point, and, consequently, the shock wave position were finely tuned to match the target by reducing the area of the underside passage, effectively shifting the balance between upper and lower mass flows.

The resulting flow field is shown in Figure 5. The flow is rapidly turned around the intake highlight and accelerates beyond the local speed of sound via expansions fans created near the front part of the intake. As these intersect the constant pressure boundary at the free-stream interface, they are reflected as compression waves, which coalesce into the physical plane to form a shock-wave. The interaction between such a shock-wave and the boundary layer, from Schlieren analysis only, appears relatively benign. No clear lambda shock pattern, characteristic of interactions resulting in flow separation, is present. The absence of a clear lambda shock wave is confirmed by LDV investigation, which shows a peak local Mach number of 1.47 in the inviscid flow region upstream of the shock. However, adverse pressure gradients characterising high incidence flight start decelerating the flow upstream of the shock, resulting in an effective Mach number immediately before the shock foot of 1.4 (Figure 6). This is somewhat beyond the generally accepted separation limit of Mach 1.3. Recirculation regions may therefore be present but confined to a small region of space, which makes their identification more challenging. Surface oil flow visualization suggests the presence of a shock-induced separation line, defined by a number of critical points, namely saddles and nodes, and three-dimensional bubbles recirculating around their foci. This is partially shown in Figure 7, which combines wall static pressure from PSP with relevant streak-lines extracted directly from oil-flow sediments. An actual photograph of the oil flow deposit on the surface is offered in the following section for comparison with the two intake variations (Figure 12b)

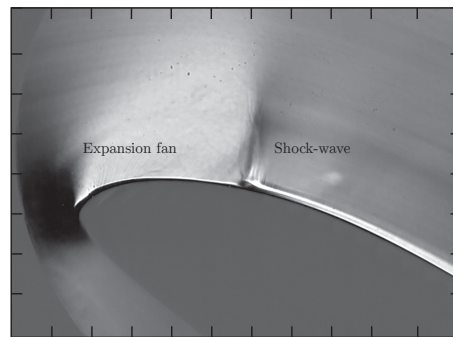
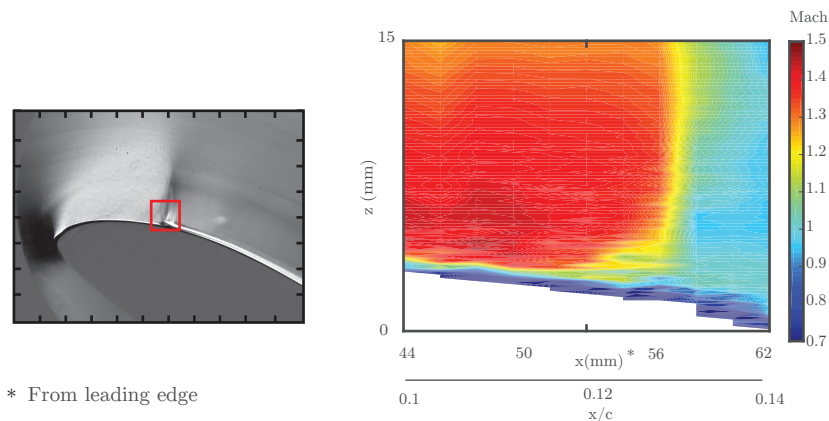


Figure 5. Schlieren photograph depicting the flow development over an engine intake lip travelling at an incidence of 23 degrees during take-off conditions. No flow image subtracted to eliminate impurities and increase contrast.



\* From leading edge

Figure 6. Local Mach number contour obtained by 12 normal LDV measurements. Noise near the wall due to difficulties in obtaining good seeding as a result of the highly curved surface.

Furthermore, the severity of the pressure jump imposed by the shock-wave, would suggest that the boundary layer might have transitioned to a turbulent nature somewhere upstream of the shock foot in order to withstand the pressure gradient.

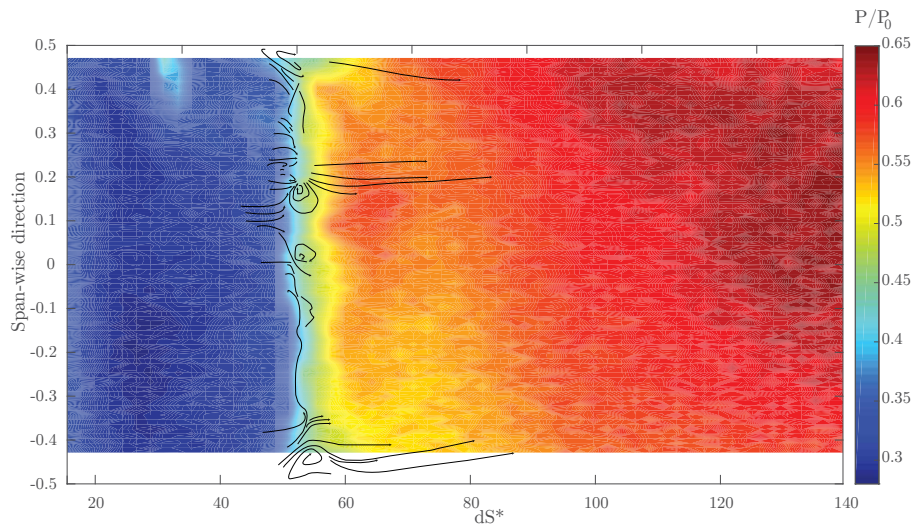


**Figure 7. Wall static pressure from processed PSP images. Black streamlines extracted from oil flow. Three dimensional bubbles appear to be localised in small region of space. Recirculation in the outer region is due to the interaction between the side-wall boundary layer and the shock.**

Overall, it can be concluded that the flow for a typical on-design case, representative of take-off conditions, is relatively benign with only small separated flow areas caused by the presence of a Mach 1.4 shock wave. This is expected to change as the mass flow demand by the engine is increased and it will be investigated in the upcoming future. The effect of varying highlight geometry will now be investigated and compared to the baseline flow.

## B. Impact of highlight (leading-edge) sharpness

The effect of varying the highlight geometry on the strength and position of the shock-wave and, most importantly, on the nature of its interaction with the incoming boundary layer will be now discussed. The stagnation pressure, relative angle of incidence and entry Mach number were kept constant, as well as the ratio between upper and lower channel.

Figure 8 shows a side by side comparison between the three different geometries characterised by an increasing highlight bluntness, defined by a greater MSE exponent. A qualitative analysis can be started based on Schlieren photographs alone. Whereas the flow that develops over the bluntest intake geometry considered appears to differ only slightly from the baseline, the shock structures characterising the sharper nose are significantly different. Here, three separate shock-waves are observed. The first sits very close to the highlight and is a consequence of the abrupt acceleration of the flow by the strong pressure gradients characterising sharp turns. The presence of a small lambda structure suggests that the interaction is separated. The flow reattaches and undergoes further acceleration before reflected expansion fans cause the second shock. The latter would appear to be of turbulent nature. However, quantitative measurements of the shock strength are required to reinforce this hypothesis. No lambda is observed. As a result of the supposedly weak shock, the flow is just below the sonic limit and becomes faster than sound again as a consequence of a third acceleration stage, which ultimately result in a third, even weaker shock wave further downstream.

The blunter nose, on the other hand, appears similar to the baseline flow. The shock position along the stream wise axis is not significantly different, which is to be expected given the similar nature of surface curvature in this region. However, a closer inspection of the interaction region shows a lambda structure appearing, suggesting a degree of boundary layer separation. The viscous layer downstream of the interaction appears to be thicker as a consequence of this. This qualitative evidence would suggest a higher Mach number at the shock foot. This hypothesis is confirmed by quantitative measurements from laser velocimetry and isentropic values from pressure readings, both of which are discussed below.

Velocity measurements were taken by means of both stream-wise readings across the inviscid region of

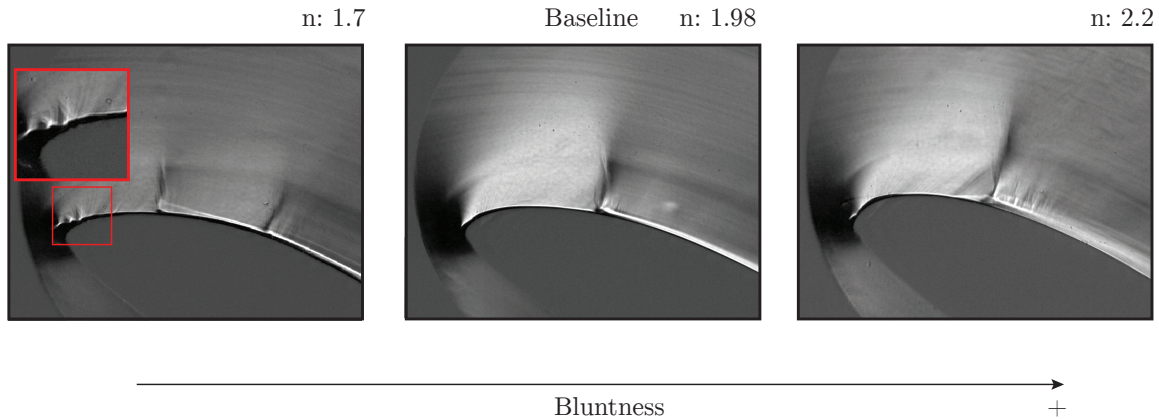


**Figure 8. Qualitative flow comparison between the three different geometries from Schlieren photography.**

the shock-wave, and by a series of normal traverses to obtain the velocity field in the shock-boundary layer interaction region. The former are depicted in Figure 9. Velocity contour plots for the region of interest of each shape are, on the other hand, depicted in Figure 10. The increased noise as the measurement volume approaches the surface is due to the difficulties encountered with seeding the flow near the wall. Improved seeding and acquisition techniques are currently being attempted with the purpose of reducing noise.

These measurements show good agreement with the velocity estimate from static pressure measurements and provide means of characterising the shock wave strength. Due to the high curvature near the sharp nose leading edge, no LDV measurement across the first interaction could be obtained. The only available measurement is a pressure tap. The location of the latter is immediately upstream of the shock-wave and recorded a value corresponding to an isentropic Mach number of 1.3. This is not expected to be able to separate a turbulent boundary layer. Thus, the interaction might be laminar. Further support to this theory comes from the extent of the interaction length. The latter is defined as the distance between the point where the incoming boundary layer starts to feel the upcoming pressure rise and the location of an ideal inviscid shock. A high value for the ratio between interaction length and the local boundary layer thickness, such as the one inferred from qualitative data, is generally associated with a laminar interaction. The central shock-wave, on the other hand, is a relatively weak Mach 1.3 shock, as measured by both stream wise traverses and velocity contours in the SBLI region. The resulting downstream velocity is just below Mach 1 and accelerates to approximately Mach 1.15 before a combination of adverse pressure gradients and a very weak final compression through a shock decelerate it to subsonic condition in the diffuser portion of the intake.

As seen from qualitative measurements, the two less aggressive blunter nose geometries, on the other hand, present only one strong shock-wave. For the baseline case ( $n=1.98$ ), the peak Mach number in the inviscid stream is just short of 1.5, before undergoing a short diffusion due to adverse pressure gradients prior to coalescence of the compression waves into  $\sim$  Mach 1.4 shock-wave. The velocity distribution in Figure 10 suggests a smeared shock foot. It is possible that there is a small lambda but this is not resolved by the measurements. In contrast, for  $n=2.2$ , corresponding to a blunter nose, a distinct lambda, albeit small in size, is reported. Similarly to the baseline case, the flow undergoes a small degree of deceleration before going through the shock. However, for the rounder nose both the peak Mach number upstream, and the one at the shock foot are higher, sitting at  $\sim 1.57$  and  $\sim 1.48$  respectively, consequence of the greater extent of favourable pressure gradient around the blunter nose.

The diffuser geometry is identical for all the variations considered and the flow velocity sufficiently downstream of the shock approaches the same velocity, just above Mach 0.9, as confirmed by both LDV (Figure 9) and static pressure measurement (Figure 11). Immediately downstream of the shock, however, the baseline and the blunter variation nose geometries show a greater degree of local flow acceleration. Shocklets are formed as a consequence of substantial acceleration over the thicker viscous layer. This is ultimately reflected in static wall pressure. Figure 11 provides a good example by depicting isentropic Mach number estimated directly from pressure sensitive paint analysis. The Mach line, highlighted in black, is substantially

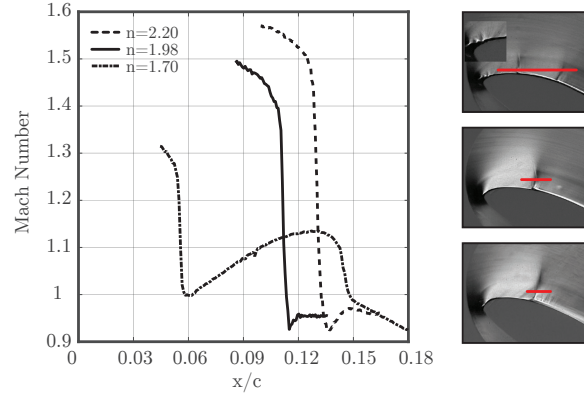


**Figure 9. Stream-wise LDV measurements across the inviscid core of the shock-wave for the three different geometries. Both the second and third compression captured for the sharper lip.**

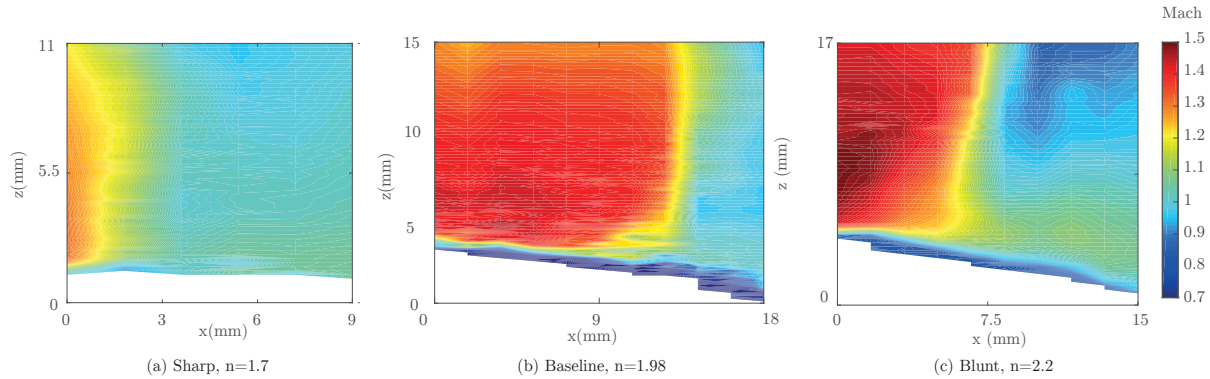


**Figure 10. Mach number contour plots of the main shock wave boundary interaction for the three different models. Mach number obtained directly from LDV measurement after temperature correction. a) depicts the central shock wave occurring over the surface of the sharp nose.**

downstream of the effective pressure jump due to the shock, reflecting the presence of a small supersonic pocket characterised by secondary shocklets. It should also be noted that both isentropic Mach from PSP and direct LDV measurements are in good agreement.

Wall static pressure, obtained from PSP analysis (Figure 11), provides a tool to assess flow two dimensionality and further strengthen the observation that side-wall effects are limited and do not greatly affect the main flow along the centreline, as anticipated in Section III A. Pressure sensitive paint images show nearly non-existent corner flows for the sharp geometry, which is consistent with a weak centre-span interaction. Similarly, recirculation regions near the wall are not found to compromise the baseline flow as these are confined to a small region of space. These tunnel effects become more evident as the centre span SBLI grows stronger, as it can be inferred from Figure 11c. Nonetheless, the corner flows are found to be dominant in less than 30% of the total span-wise distance and are not thought to have major impact on the extent of centre-span separation. Oil flow visualization offers a clearer depiction of the vortical structures characterising corner flows for both the baseline and the blunt nose (Figure 12b and 12c) and strengthens the assumption of negligible impact of wind-tunnel effect on centre-span separation onset. On another hand, oil flow also confirms the presence of shock-induced separation lines for two of the three geometries considered. As depicted in Figure 12b, the baseline flow streak lines present a distinct separation line defined by saddle and nodal points in correspondence with the location of the shock-wave. Whereas this is a fairly two dimensional attribute, the reattachment appears to be dominated by three-dimensional features. A number of owl-face separations are present, with four foci clearly distinguishable. The reattachment lines at those

span-wise locations where owl-face separations are not present are not clearly captured by the oil mixture. The blunter nose shows similar flow features. Overall, separation appears more pronounced for the blunter geometry, which is consistent with the other measurements. Finally, for the sharpest intake geometry, shock induced separation is present in the form of extremely small bubbles in the immediate proximity of the highlight. A subtle saddle point would appear to be present in the centre-span, as a result of the second shock-wave. The reattachment line is not distinguishable but believed to be immediately downstream of the separation point.

## IV. Conclusion

The flow development around an aero-engine intake travelling at an incidence has been investigated and the results for a baseline case and two geometry variations are presented here. The baseline flow, for which target was provided by 3D CFD on nacelles, showed a shock-wave boundary layer interaction with a strength of  $M=1.4$ , which is around the onset of shock induced separation. Oil flow visualisation suggests that a small separation exists in the form of small, localised, 3D pockets. Two leading edge geometries have been tested for equivalent flow conditions. The experimental measurements reveal a substantial influence of near-leading edge curvature on the supersonic flow development. Compared to the baseline case, a sharper nose results in strong local acceleration, which leads to a first terminal shock in the immediate proximity of the leading-edge. The flow undergoes two further re-acceleration stages, both terminated by shock waves of decreasing intensity. The flow shows an exceptional two-dimensionality and separation bubbles are absent for the two SBLI occurring over the upper part of the lip. Conversely, the favourable pressure gradients characterising blunter noses favour the development of a larger supersonic region, terminated by a stronger shock, which appears to be associated with a degree of flow separation. At this stage stagnation pressure recovery has not yet been measured. However, there is sufficient evidence to support the hypothesis that a sharper nose would reduce the wave drag losses as compression occurs via a number of shock, thus closer to an isentropic phenomena.

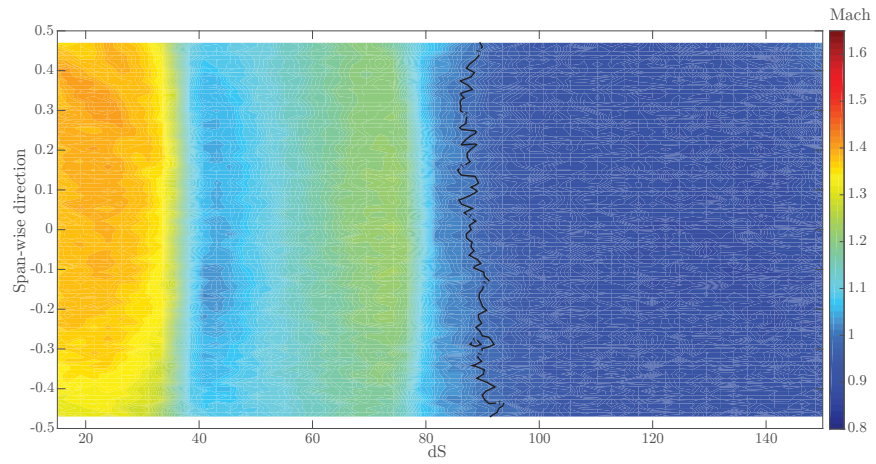
Nonetheless, for the flow conditions considered in the current investigation, chosen to investigate the interaction between the shock and the boundary layer during typical high incidence manoeuvring, appear to be relatively benign for all of the shape considered. Ultimately, none of them showed inherently unsteady characteristics associated with largely separated flows. Future research will try to assess the onset of unsteadiness before attempting its control.

## Acknowledgements

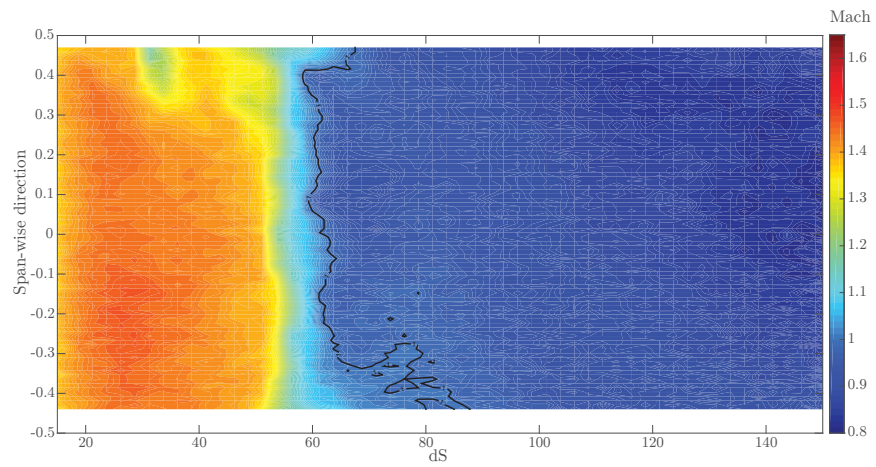
The authors wish to acknowledge David Martin, Sam Flint, Anthony Lockett and John Hazlewood for operating the CUED blow-down wind tunnel and Kevin Bullman for the manufacturing of the models used in this investigation. Moreover, they would like to thank Rolls Royce Plc and the Engineering and Physical Sciences Research Council (EPSRC) for funding the current research.

## References

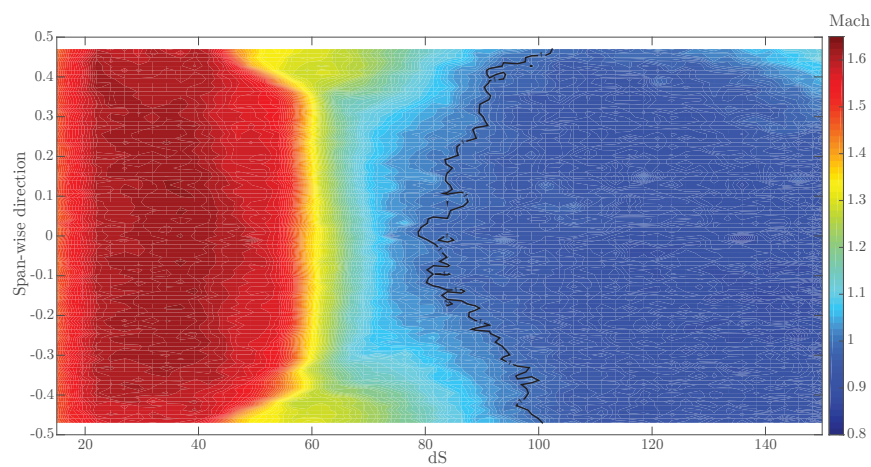
- <sup>1</sup>DAGGET, D. L., BROWN, S. T., and KAWAI, R. T., "Ultra-Efficient Engine Dimaeter Study," *NASA Technical Report No. 212309*, 2003.
- <sup>2</sup>MAKUNI, T. E., *Experimental Investigations of the Interaction between Normal Shock Waves and Transitional Boundary-Layers in Subsonic Intakes at High Incidence*, First Year Report, University of Cambridge, august 2013.
- <sup>3</sup>FERRI, A., *Elements of Aerodynamics of Supersonic Flows*, Macmillan Co., 1949.
- <sup>4</sup>GREGORY, J. W., ASAI, K., KAMEDA, M., LIU, T., and SULLIVAN, J. P., "A review of pressure-sensitive paint for high-speed and unsteady aerodynamics," *Proc. IMechE Vol. 222 Part G: J. Aerospace Engineering*, 2007.
- <sup>5</sup>LIN, N., REED, H. L., and SARIC, W. S., "Effect of leading-edge geometry on boundary-layer receptivity to freestream sound," *Instability, Transition, and Turbulence*, 1992, pp. 421–440.
- <sup>6</sup>SCHRADER, L.-U., BRANDT, L., MAVRIPIIS, C., and HENNINGSON, D. S., "Receptivity to free-stream vorticity of flow past a flat plate with elliptic leading edge," *Journal of Fluid Mechanics*, Vol. 653, 2010, pp. 245–271.
- <sup>7</sup>BRUCE, P. J. K., BURTON, D. M. F., TITCHENER, N., and BABINSKY, H., "Corner effect and separation in transonic channel flows," *Journal of Fluid Mechanics*, Vol. 679, 2011, pp. 247–262.



(a) Sharp highlight,  $n=1.7$ .



(b) Baseline,  $n=1.98$ .

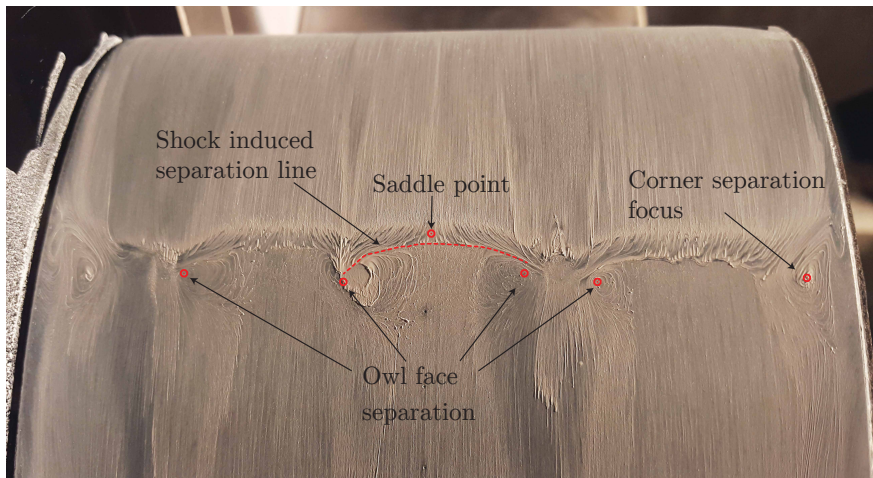


(c) Blunt highlight,  $n=2.2$ .

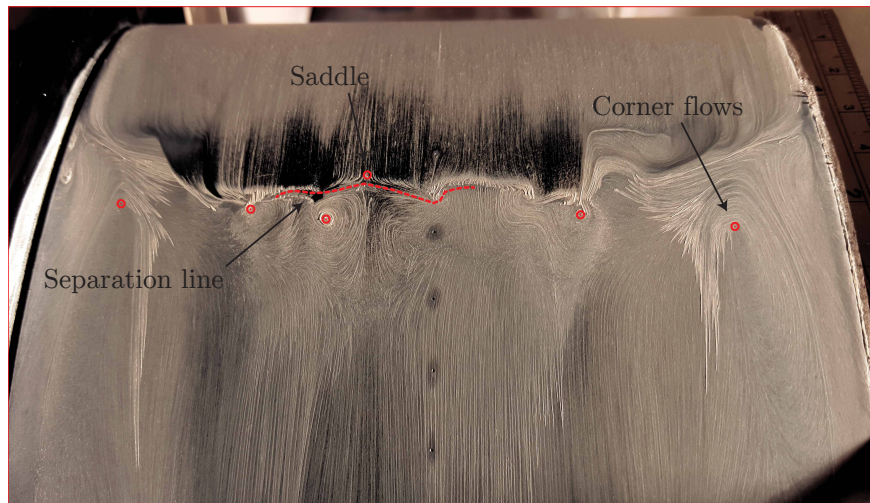
Figure 11. Comparison between isentropic Mach number calculated from wall static pressure along the model surface measured from PSP. Mach line highlighted in black. Top right corner and b) affected by poor lighting.



(a) Sharp highlight,  $n=1.7$ .



(b) Baseline,  $n=1.98$ .



(c) Blunt highlight,  $n=2.2$ .

Figure 12. Oil flow visualization image. Pressure tap located at identical stream wise positions.